Controlled switching of 10-micrometer radiation using semiconductor étalons

P. B. Corkum and D. Keith*

Division of Physics, National Research Council of Canada, Ottawa, Ontario K1A OR6, Canada

Received March 29, 1985; accepted July 26, 1985

An 80-MHz train of pulses, each lasting ~200 psec, has been switched from the output of a ~1-W cw CO_2 laser. The switching element, an uncoated Cr-doped GaAs étalon, was controlled by the ~1-W average power output of an argon-ion laser. Sensitive picosecond switching, pulse differentiation, and contrast enhancement of 10-μm pulses are also demonstrated using high-finesse étalons. The sensitivity of plasma-based devices for the control of ~10-μm and longer wavelength radiation is emphasized, and the physics of a new device (a plasma-beam deflector) is discussed.

1. INTRODUCTION

The development of picosecond pulses in the visible and near infrared has been based largely on improvements in mode-locked lasers. These techniques cannot easily be transferred to the mid-infrared. For the generation of picosecond pulses in the mid-infrared, nonlinear methods have usually been used along with high-power, short-wavelength picosecond sources.[1–3] In the only published work for which a picosecond, short-wavelength source was not required, a high-power ($\simeq 10^7$-W) mid-infrared pulse was necessary.[4] The high power required from at least one laser involved in the generation of picosecond mid-infrared pulses has placed a severe restriction (to ~1000 Hz) on the repetition rate at which picosecond mid-infrared pulses can be generated.

The development of high-repetition-rate sources of picosecond pulses in the mid-infrared would be desirable. For example, it should be possible to apply noise-reduction techniques similar to those that have been developed for cw mode-locked dye lasers. Furthermore, if the pulses are phase coherent (see Section 5), heterodyne or other phase-sensitive techniques should be applicable. Also, recent advances in optical fibers suggest that long-distance optical communications systems may eventually operate in the mid-infrared.[5] Simple, high-repetition-rate sources of picosecond pulses will be required for these applications.

Of all the techniques for the generation of picosecond mid-infrared pulses that have been demonstrated, it is optical switching[1] that promises the lowest-power operation. This is because parametric techniques[2,3] require long interaction lengths for the mid-infrared pulse to grow from noise. Consequently, relatively large interaction areas are necessary. Large interaction areas have, however, characterized previous work with optical switching as well. For optical switching with étalons, on the other hand, the beam cross section can be small, enabling the total energy required in the control pulse to remain low. The small size implies that the device can be easily cooled, and this suggests that higher average powers per unit area can be used.

In addition to demonstrating optical switching using étalons, this paper will show that étalons can be used to increase the signal-to-background contrast of switched, picosecond pulses (contrast enhancement) and to decrease passively the time duration of a fast rise time, relatively long switched pulse (pulse differentiation). The outline of the remainder of the paper is as follows.

Section 2 examines the general importance of plasma nonlinearities for the control of mid-infrared (and longer-wavelength) radiation.

Section 3 deals with the response of étalons to picosecond pulses. Equations are derived to describe the switching of infrared radiation using semiconductor étalons by optically injected plasmas.

Section 4 is devoted to experimental observations. Subsection 4.A describes large-area étalon switching on Si substrates. The subject of Subsection 4.B is the experimental generation of a cw train of ~200-psec 10-μm pulses at a repetition rate of 80 MHz. In Subsection 4.C we demonstrate the use of étalons for contrast enhancement and differentiation.

In the concluding section we discuss some of the implications of étalon switching as well as applications of plasma nonlinearities to a proposed infrared streak camera.

2. PLASMA NONLINEARITY

Nonlinear optical devices are based on refractive-index changes ($\delta\eta$) experienced by a pulse, as a result of either an external perturbation or the pulse itself:

$$\eta = \eta_0 + \delta\eta. \tag{1}$$

In almost all cases the nonlinearity is due to bound electrons. This is true for Pockels cells, electro-optic beam deflectors, many optically bistable devices, and optical pulse compression (frequency-chirping) systems used in the visible. In all these devices $\delta\eta$ can be described by

$$\delta\eta = \eta_i E_i + \eta_{ij} E_i E_j + \ldots. \tag{2}$$

In general, nonlinear devices operate by modifying the wave front of a beam. For a given phase shift, the parameter $\delta\eta/\lambda$ must be kept constant as the wavelength is changed. Under some circumstances this wavelength scaling can be useful for infrared applications. For example, self-focusing

0740-3224/85/121873-07$02.00

is much less severe in the infrared. Partly for this reason, infrared lasers can operate at higher power densities than can lasers in the visible. For devices, however, the wavelength scaling is not an advantage.

Although electronic nonlinearities have been used in virtually all electro-optic devices, $\delta\eta$ associated with plasmas has an explicit wavelength dependence that more than counteracts the $1/\lambda$ behavior of the parameter $\delta\eta/\lambda$. This is illustrated by the following equation for the refractive index of a plasma:

$$\eta = \eta_0\left(1 - \frac{N_e}{N_{cr}}\right)^{1/2}. \tag{3}$$

In Eq. (3) N_e is the electron (or free-carrier) density and N_{cr} is the critical density. The critical density is defined as

$$N_{cr} = \frac{\omega^2 m \eta_0^2}{4\pi e^2}, \tag{4}$$

where ω is the angular frequency of an electromagnetic wave of wavelength λ, m is the free-carrier (electron) reduced mass, and e is the electronic charge. From Eq. (4) it is clear that $N_{cr} \propto \lambda^{-2}$.

For free-carrier densities $N_e \ll N_{cr}$, Eq. (3) can be expanded as

$$\eta = \eta_0 - \tfrac{1}{2}\eta_0\frac{N_e}{N_{cr}} + \ldots. \tag{5}$$

We can then make the obvious correspondence between the terms $(\eta_i E_i + \eta_{ij}E_iE_j + \ldots)$ and $(\eta_0 N_e/2N_{cr} + \ldots)$.

It is clear that, whereas the nonlinear terms in Eq. (2) are not explicitly dependent on the wavelength, the corresponding plasma terms have an explicit λ dependence through N_{cr}.

It is constructive to compare the magnitude of these two terms. As an example, consider CS_2, a highly nonlinear liquid used for frequency chirping and for Kerr cells. For CS_2, the nonlinear coefficients are given by $\eta_i = 0$ and $\eta_{ij} = \eta_2\delta_{ij}$, where $\eta_2 = 2.2 \times 10^{-20}\ \mathrm{m^2\ V^{-2}}$. Using a typical applied field of 10 kV/cm, we obtain a value of

$$\delta\eta = \eta_2 E^2 = 2.2 \times 10^{-8}.$$

For a free-carrier plasma in GaAs, $\eta_0 = 3.5$ and $N_{cr} \sim 10^{19}\ \mathrm{cm^{-3}}$. Assuming 10-$\mu$m radiation and an electron density of $N_e \sim 10^{15}\ \mathrm{cm^{-3}}$ (of course, much higher densities can be optically injected), these parameters yield

$$\delta\eta = \frac{\eta_0 N_e}{2N_{cr}} = 1.7 \times 10^{-4}.$$

The same electron density in InSb would yield $\delta\eta \sim 2 \times 10^{-3}$. Thus even at these very low electron densities, $\delta\eta$ of semiconductors can be 5 orders of magnitude larger than that of CS_2.

As a final comparison, GaAs is also a material with a large first-order nonlinear coefficient (GaAs is used extensively for Pockels cells in the 10-μm region). We can compare the electronic nonlinear response of GaAs ($\eta_i = 5.8 \times 10^{-11}\ \mathrm{m/V}$) with the plasma nonlinearity in the same material. For a field strength of 10 kV/cm $\delta\eta = 5.8 \times 10^{-5}$.

Of course, the nonlinear term in Eq. (5) is not explicitly nonlinear. However, the parameter N_e or N_{cr} can be modified either by the pulse itself or by an external field. In other words, N_e and N_{cr} are, in many cases, implicitly dependent on the fields.[6]

There are many different approaches to modifying the plasma density or the critical density and, as with electronic nonlinearities, these can lead to a wide array of possible devices.

3. THEORY OF ÉTALON SWITCHING

In the steady state, the reflection (R) and transmission (T) of an ideal étalon illuminated by an infinite, normally incident plane wave is given by

$$R = \frac{r(1 - 2t\cos\delta + \delta + t^2}{1 - 2rt\cos\delta + r^2t^2}, \tag{6a}$$

$$T = \frac{(1-r)^2 t}{1 - 2rt\cos\delta + r^2t^2}. \tag{6b}$$

In these equations, r is the reflectivity of each étalon surface (assumed to be equal), $t = (1 - A)$, where A is the single-pass absorption of the étalon, and δ is the phase change of the incident radiation over one round trip through the étalon. By modifying any of these parameters, the reflectivity R and the transmission T of the étalon can be modified (switched).

For switching, we consider the case in which $R \sim 0$. This implies that $t \sim 1$, $\delta \sim 2n\pi$, where n is a positive integer greater than 0. To determine the change in reflectivity caused by change in δ and/or t, we can perform a Taylor expansion of Eq. (6a) about the point $R = 0$. For simplicity, consider the case where the surface reflectivity r is fixed. The resulting equation gives

$$dR = \frac{2r}{(r-1)^2}(d\delta^2 + dt^2). \tag{7}$$

It is obvious from Eq. (7) that an étalon's sensitivity as a switch increases with increasing surface reflectivity. However, in choosing the surface reflectivity, one must find a balance between an acceptable background level and the sensitivity of the étalon.

The transient response of an étalon is governed by the photon cavity lifetime. It is given by

$$\tau = \frac{\eta L}{c[\ln(rt)]}, \tag{8}$$

where L is the étalon thickness. In the continuous approximation, if a step-function change is made in the conditions of the étalons or in the incident light, the reflected and transmitted intensity will exponentially approach a new steady-state value with this time constant.

This transient response of an étalon can be exploited to reflect short pulses selectively. Thus an étalon tuned to a minimum reflectivity acts as a differentiator from which changes in light intensity that occur on a time scale less than τ are reflected, while slowly changing radiation is transmitted. We demonstrate this effect for fast rising pulses in Section 4. (Pulses with fast fall times generated by gas breakdown have been used previously to make short pulses using this effect.[7])

In previous work étalons have been used in optically bistable devices.[8] In our experiments, we control étalons' reflectivity at 10 μm by using above-band-gap radiation to form a semiconductor plasma in the étalon, which in turn changes the refractive index.

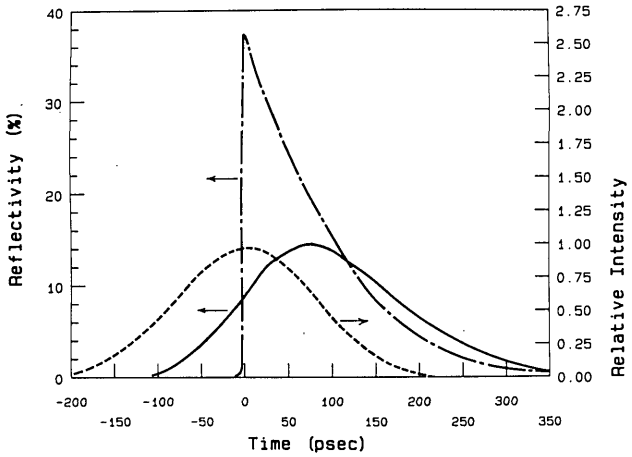

Fig. 1. Calculated response of the 10-μm reflectivity (left axis) of a Cr:GaAs étalon initially tuned to minimum reflectivity. The solid curve was calculated assuming that the étalon was illuminated with the 200-psec, 514-nm control pulse shown by the dashed curve (right axis) and assuming an absorbed fluence of 60 μJ/cm^2. Also shown is the calculated response for a 1-psec, 0.6-μm control pulse containing the same absorbed fluence.

Injection of a plasma of carrier density N_e modifies the phase δ by an amount $\Delta\delta$ over each round trip:

$$\Delta\delta = \frac{2\pi\eta_0}{\lambda_v N_{cr}} \int N_e dl, \tag{9}$$

where λ_v is the vacuum wavelength of the incident wave.

The transmission (t) of the below-band-gap radiation is also modified:

$$\Delta t = 1 - \exp(-\alpha \int N_e dl), \tag{10}$$

where α is the free-carrier absorption cross section.

By combining Eqs. (4) and (9) above, we can re-express $\Delta\delta$:

$$\Delta\delta = \frac{2e^2}{c^2\eta_0} \frac{\lambda_v}{m} \int N_e dl. \tag{11}$$

From Eq. (11), we see that, for a given $\int N_e dl$, the phase change is proportional to λ_v and inversely proportional to the carrier reduced mass.

For typical semiconductor étalons and small plasma densities, the change in phase $\Delta\delta$ is larger than the change in the transmission of Δt. For example, in the case GaAs in the limit of small $\int N_e dl$ (less than 5×10^{14} cm^{-2}) we have $\Delta\delta/\Delta t \sim 14$.

In Fig. 1, we plot the calculated response of the 10-μm reflectivity of a GaAa étalon that is tuned to a null. Using the known free-carrier lifetime (measured by photoconductivity), results are presented for two experimental conditions.

(1) The dashed curve plots an incident (control) 514-nm pulse of 180-psec duration. This is a pulse similar to that used in an experiment that we describe in the following section. The solid curve shows the calculated time dependence in the 10-μm reflectivity resulting from a control pulse with an absorbed fluence of 60 μJ/cm^2.

(2) Also plotted is the time dependence of the 10-μm reflectivity expected for a picosecond (delta-function) pulse with the same fluence.

4. EXPERIMENTAL OBSERVATIONS

Experiments were performed with two different 10-μm sources, one a hybrid CO_2 laser, line tunable and operating on a single transverse and longitudinal mode, the other a cw CO_2 laser with a maximum output of ~1 W. Two visible sources were also used, one a 2-psec, 616-nm pulse with energy as high as 1 mJ per pulse and the other the 514-nm output of a cw mode-locked argon-ion laser. Five different étalons were used: two 90-μm-thick Si étalons, one uncoated and the other coated with a surface reflectivity of 92% at 10 μm; two 300-μm-thick Ge étalons, one uncoated and the other coated for a surface reflectivity of 82%; and an 100-μm-thick uncoated Cr-doped GaAs (Cr:GaAs) étalon.

Different étalon materials were required because of the different fabrication and semiconductor properties of each. The penetration depth of 616-nm light in Si is relatively large (~2 μm), and the recombination time in our intrinsic sample was long ($\tau > 1$ μsec). Thus an infrared pulse switched on a Si étalon using a picosecond control pulse will have a fast rise and a very long decay time. A similar recombination time is expected for bulk Ge, but the small penetration (20-nm) depth of 616-nm light in Ge implies that surface properties will be important. For this reason we have not investigated Ge switching. The penetration depth of Cr:GaAs at 5145 nm is likewise very small (~100 nm). In preparation the GaAs surface was optically polished and simultaneously etched, but surface recombination may still lead to a reduced free-carrier concentration and faster recombination than we might otherwise expect. (This has not been accounted for in Fig. 1.)

A. Silicon Étalon

To demonstrate étalon switching in the simplest possible configuration [Fig. 2(a)], we used the high-reflectivity Si étalon. The high-power 10-μm pulse was incident at a power density of ~2×10^6 W/cm^2, illuminating an area of 0.04 cm^2. Even when adjusted for minimum reflectivity, an unswitched residual background of 5% was measured. This background was mainly due to the 10-μm absorption of the Si substrate.

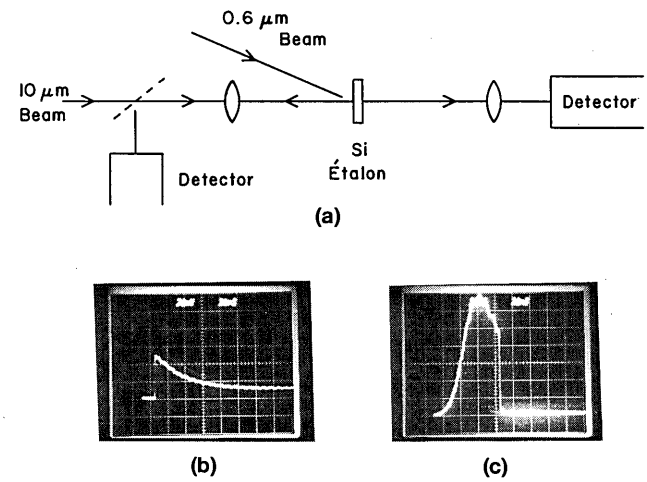

Fig. 2. High-power switching on a Si étalon. (a) Schematic of experimental configuration. (b) The change in the infrared reflectivity and (c) transmission of the étalon as the result of a high-power (~5-mJ/cm^2) 616-nm control pulse. The horizontal scale is 20 nsec/division.

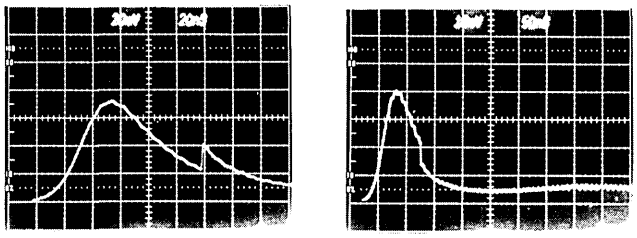

Fig. 3. Oscilloscope traces illustrating that the infrared reflectivity of Si étalons can be controlled by very-low-power 616-nm radiation. (a) An étalon, initially at minimum reflectivity is moved off resonance by the same power density control pulse. (b) An étalon only slightly too thick is moved nearer to null reflectivity by the 10-μJ/cm^2 absorbed 616-nm control pulse.

The 2-psec 0.6-μm control pulse contained an energy as high as 1 mJ. The response of the étalon is shown in Figs. 2(b) and 2(c) for an incident energy density of $\sim$5 mJ/cm^2. At this intensity, so many carriers are optically injected that a strongly absorbing plasma is created. Under these conditions, the étalon reflectivity must switch to its front surface reflectivity of 92% in the 2-psec duration of the control pulse. The reflectivity, as measured by comparison with the 5% background level, is 90 $\pm$ 10%.

In Section 3 we predicted that at lower intensity the change in the optical path length of the étalon should dominate the change in reflectivity of an étalon. This is demonstrated in Figs. 3(a) and 3(b), where an incident energy of 10 μJ/cm^2 of 0.6-μm radiation is used. A small wedge angle on the étalon allowed its thickness to be tuned to either side of the reflectivity minimum. If an étalon is slightly too thick, the injection of free carriers (which decreases the refractive index) will move the étalon closer to resonance and consequently decrease the reflectivity [Fig. 3(a)]. For an étalon, either at resonance or too thin, free-carrier injection increases the étalon reflectivity [Fig. 3(b)]. Figure 3(b) is an oscillogram of the 10-μm reflectivity of an étalon, initially on resonance. The observed reflectivity changes from the baseline value of $\sim$5% to a peak value of $\sim$10%, in qualitative agreement with Eqs. (7) and (11).

Thus we demonstrate two modes of operation. One is based on controlled absorption and the other on changes in the optical path length of the étalon. Although both effects are always present, optical-path-length switching dominates at low illumination levels, absorption switching at high intensities. The former has a response time of the photon cavity lifetime of the étalon, while switching based on sufficiently strong absorption can be virtually instantaneous. Like semiconductor reflection switching, étalon switching based on absorption seems destined to be scalable well into the subpicosecond time scale.[9]

B. Continuous-Wave Trains of 10-μm Pulses

Having demonstrated that 10-μm switching is possible with control pulses containing as little as 10 μJ/cm^2 of above-band-gap radiation, it is possible to consider the use of very-low-power picosecond control sources.

Perhaps the most important of these are cw mode-locked lasers. Typically, they contain single pulse energies of between 1 and 10 nJ/pulse. Such energies are more than sufficient to control even low-finesse étalons over significant areas ($\sim 10^{-4}$ cm^2). We have chosen to modulate the beam produced by a 1-W cw CO_2 laser with the output of an 0.8-W cw mode-locked (81-MHz) argon-ion laser operated on the 514-nm transition. The argon laser has a measured pulse duration of 180 psec.

The experimental arrangement is shown in Fig. 4. The low-pressure (20-Torr) CO_2 laser was tuned to a single rotational line. The beam was spatially filtered, passed through a 50% beam splitter, and focused by a 6-cm focal-length $F/4$ lens at normal incidence onto a 100-μm-thick Cr:GaAs étalon. Any backreflected radiation was recollimated; 50% was reflected from the beam splitter and monitored on a 300-MHz HgCdTe detector.

To reduce heat loading and to aid in detection, both beams could be chopped at 50 Hz with a duty cycle of 200:1. The background reflectivity was $\sim 10^{-3}$ in the true cw mode, although to obtain this reflectivity the étalon had to be tuned to minimum background while it was being illuminated. A small wedge aided tuning. When the beam was chopped, the rapidly changing temperature of the étalon increased the background to $\sim 10^{-2}$.

The contrast between the short switched pulses and the background radiation was further increased using a hot CO_2 cell. In hot CO_2, the narrow-bandwidth background radiation is absorbed while the broad-bandwidth short pulses are transmitted with little attenuation. The hot cell that transmitted only 10% of the narrow-bandwidth background radiation was operated in the range 10–70 Torr.

The upper traces in Fig. 5 show a trace of the (unchopped) cw train of 10-μm pulses. These pulses are bandwidth limited on the detector–oscilloscope combination. Because of saturation of our detector, the true pulse height and background level cannot be accurately determined. The fluctuations in pulse height observed in Fig. 5(b) are due to fluctuations in the pulse energy from the argon-ion laser. Cw trains of picosecond pulses were observable with control pulse energies as low as 0.25 nJ.

Figure 5(c) shows the photoconductivity of the same Cr:GaAs sample used to fabricate the étalon. This was obtained by depositing a 50-Ω strip line on the GaAs substrate in a manner similar to that described by Auston *et*

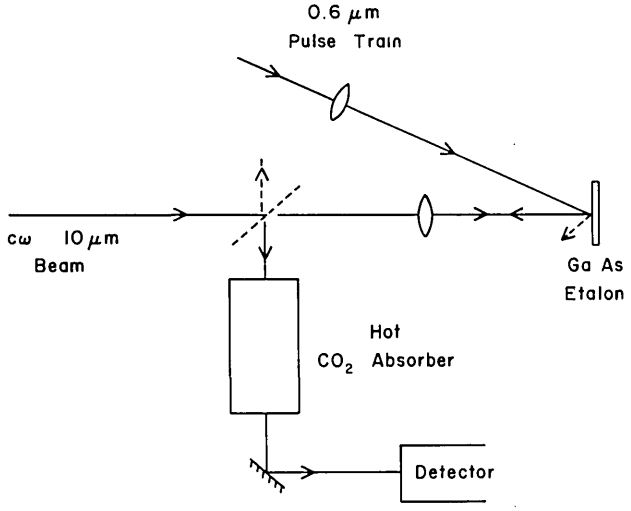

Fig. 4. Experimental configuration used to generate cw trains of 10-μm pulses.

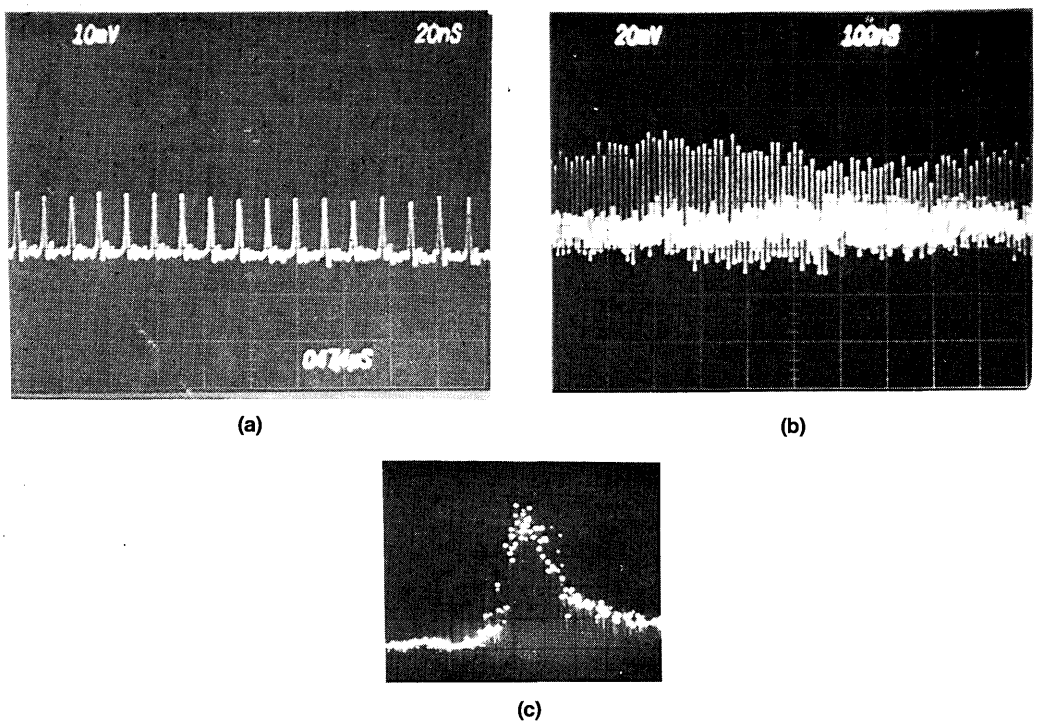

Fig. 5. Oscilloscope traces illustrating the generation of cw trains of 10-μm pulses. (a) and (b) Train of subnanosecond 10-μm pulses shown on different time scales. The pulse separation is 12 nsec. (c) Photoconductive response of the GaAs substrate to a picosecond 616-nm pulse. The total trace width is 850 psec.

al.[10] Under low-intensity illumination the conductivity is proportional to the free-carrier density. Thus the decay of the photoconductivity after free-carrier injection can be used to determine the free-carrier lifetime. The free-carrier recombination rate obtained in this manner was used to calculate the étalon time response shown in Fig. 1. It provides our best evidence that the 10-μm pulse duration is ~200 psec.

C. Contrast Enhancement and Pulse Differentiation

For reproducible pulses, optical switching requires that the incident mid-infrared beam be unmodulated on the time scale of the jitter between the infrared and control laser pulses. Thus, in most cases, any unswitched (background) radiation has a narrow linewidth and can ideally be discriminated against with a resonant structure such as an étalon.

Although contrast enhancement is useful in picosecond systems, a short pulse reflected from an étalon will have its temporal structure changed. For example, the pulse in Fig. 2(a) would have the prepulse background suppressed, and, since the reflected pulse is long compared to the photon cavity lifetime, after some transient response, the latter parts of the pulse must also be suppressed. Only the fast transient can be reflected. This is shown in the oscilloscope traces in Fig. 6 obtained using a 300-MHz HgCdTe deflector. To obtain the right trace, the pulse shown in the left trace was reflected from the r = 82%, 300-μm-thick Ge étalon adjusted for background suppression. Since the photon cavity lifetime of this étalon is $\tau \sim 40$ psec, the reflected pulse must have a similar duration.

Although Fig. 6 provides a graphic demonstration of contrast enhancement and pulse differentiation, it is possible to

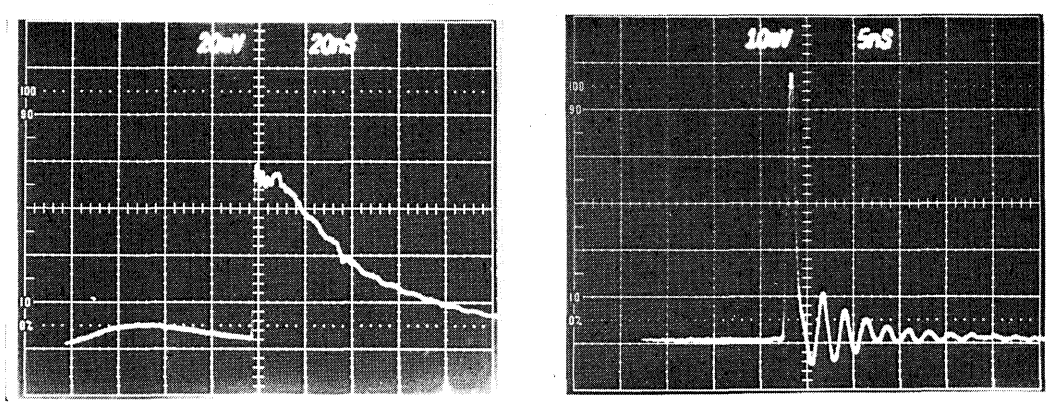

Fig. 6. Oscilloscope traces illustrating pulse differentiation. Left trace: An incident 10-μm pulse generated as in Fig. 2. Right trace: A single pulse produced by reflecting this pulse off a 300-μm-thick, r = 80% germanium étalon. The étalon was adjusted for null background reflectivity. The horizontal scale is 5 nsec/division.

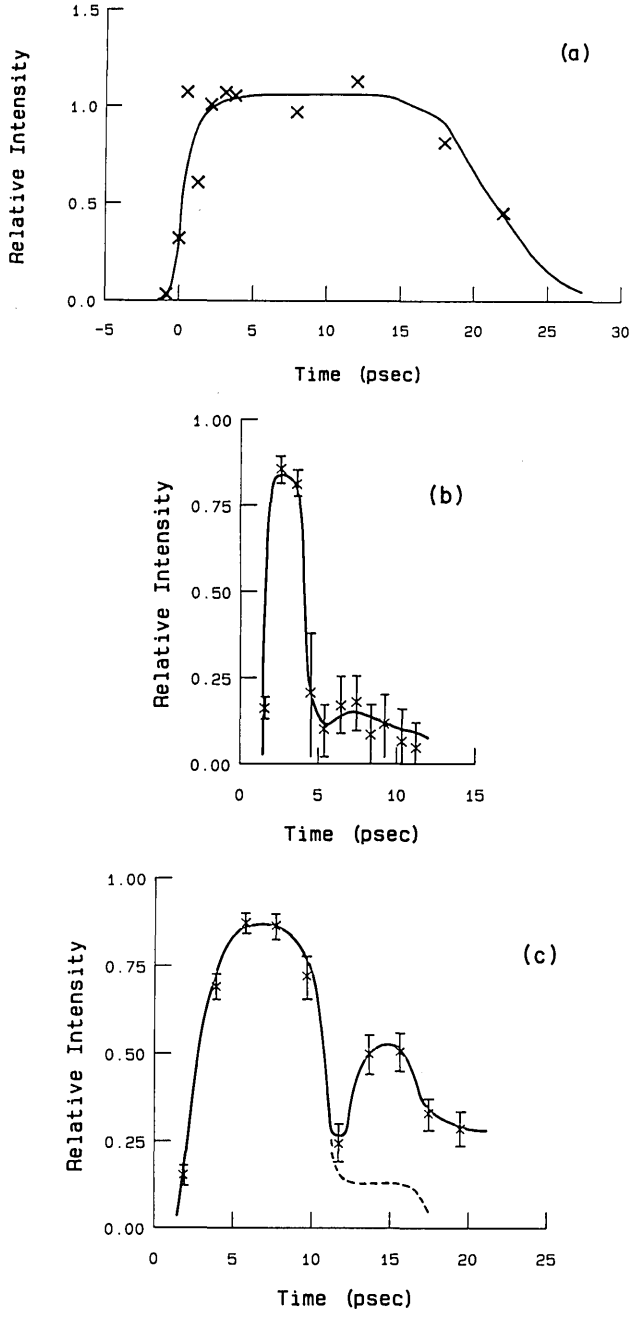

Fig. 7. An incident pulse (a) generated by semiconductor reflecting switching is differentiated by reflecting from a 300-μm Ge étalon (c) or a 70-μm Si étalon (b). Both étalons were adjusted for minimum reflectivity of the background radiation. The dashed curve in (c) is the signal expected for an unchirped pulse.

make time-resolved measurements of a pulse reflected from a thin étalon. In a previous experiment[9] using semiconductor reflection switching on GaAs substrates, we have been able to measure the time duration of the reflected pulse switched under the control of a 2-psec pulse of 0.6-μm light. This pulse can be used to investigate the transient response of an étalon, and, conversely, the étalon can be used to investigate the chirp that must be impressed on this pulse by the time dependence of the free-carrier plasma density in a Cr:GaAs semiconductor switch.

Figure 7(a) is a plot of the pulse shape made by semiconductor reflection switching. The pulse rise time of ~2 psec and near-constant intensity makes it a good pulse for investigating pulse differentiation with étalons. The use of this pulse in a high-power laser system has been described in Ref. 9, as was the pulse measurement technique that we have used.

Figure 7(c) is a plot of the reflected pulse from a 300-μm uncoated Ge étalon. A large-amplitude 8-psec component, characteristic of the transit time in the Ge, is clearly evident. However, for 8 psec $< t <$ 20 psec reflected intensity is greater than expected (dashed curve) for a constant-intensity nonchirped pulse. This is due to the small chirp that is known to be produced by a reflecting plasma with a rapidly changing density. It is not possible to compare these results quantitatively with the predictions of Ref. 1, which were calculated for a semi-infinite plasma. In the present experiment, the relatively small thickness (~3000 Å) of the optically injected plasma layer and the time dependence of the layer thickness are additional complications.

Decreasing the round-trip time of the étalon will decrease the background signal, since, for a linear chirp, the interfering components have had less time for phase changes to build up. This is demonstrated in Fig. 7(b), where a 70-μm uncoated Si étalon was used. Clearly evident in Fig. 7(b) is a high-intensity 2-psec structure due to the front surface reflectivity alone followed by a low-intensity component. Experimentally, we find that ~60% of the energy reflected from the étalon is in the 2-psec spike, with the remaining 40% accounted for in the low-energy tail. This implies a signal-to-background power contrast of ~30:1.

5. DISCUSSION

We have demonstrated that semiconductor étalons can serve as sensitive optical switches for mid-infrared radiation. By showing that they can be controlled by above-band-gap pulses containing an energy of less than 1 nJ, we have demonstrated that even semiconductor laser sources can, or will soon be able to, control infrared optical switches. In fact, we estimate that with InSb as a substrate material, a high-finesse étalon can be modulated with as little as 1 pJ. This has important implications for simple sources of picosecond (or longer) pulses in the mid-infrared.

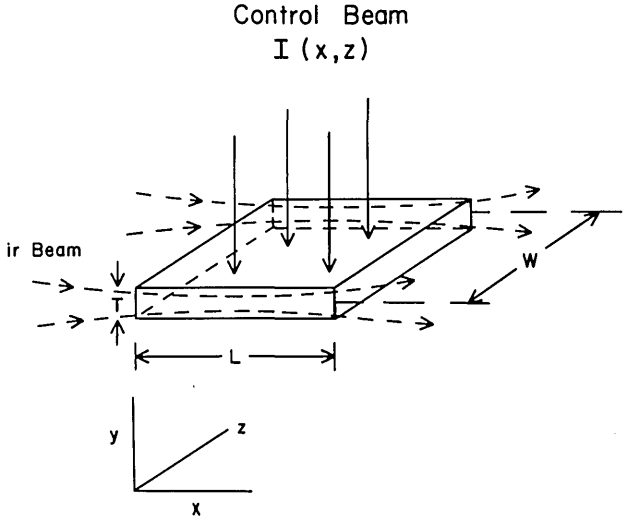

Fig. 8. Schematic representation of an infrared beam deflector controlled by above-band-gap radiation.

Étalon switches also have major advantages over other types of optical switches for some long-pulse (nanosecond to microsecond) applications. As is clear from Fig. 6, the same control energy that can generate a picosecond pulse is also sufficient to operate a microsecond switches.

We have also developed the first reported cw train of subnanosecond mid-infrared pulses. Since it is generated by switching portions from a narrow-linewidth CO_2 laser (such lasers can have bandwidths as small as $\Delta\nu < 2000$ Hz), the pulses are, or can be, phase coherent with each other as well as with the incident, unmodulated beam. Thus, aside from the obvious pulse-probe experiments that can arise from the synchronization of the cw visible and 10-μm sources, picosecond phase-sensitive experiments can be performed.

In addition, we have discussed the more general concept of plasma nonlinearities and emphasized its correspondence with the more traditional electronic nonlinearities. This correspondence suggests a number of new devices, perhaps the most important of which is a plasma-beam deflector. We will briefly illustrate this.

Electro-optic beam deflectors have been rather extensively investigated in the visible.[11,12] We can describe the corresponding plasma device by considering an infrared beam confined near the surface of a semiconductor (Fig. 8).

If the above-band-gap radiation is absorbed uniformly across the thickness T, with an absorbed fluence of $E(z) = z\int I_0(t, x)\mathrm{d}t$ and producing one carrier pair per absorbed photon, then the phase retardation by the end of the pulse can be written as

$$\delta\phi(z) = \frac{1}{2}\frac{\eta_0}{\lambda_v}\frac{z\int_0^L\int_{-\infty}^{\infty} I_0(t,x)\mathrm{d}t\mathrm{d}x}{h\nu TN_{cr}}. \tag{12}$$

In Eq. (12) $h\nu$ is the photon energy of the above-band-gap radiation.

For $I_0(t, x) = I_0$ in the interval $0 < t < \tau$, and $I(t, x) = 0$ otherwise, Eq. (12) simplifies to

$$\delta\phi(z,t) = \frac{1}{2}\frac{\eta_0}{\lambda_v}\frac{I_0 L}{h\nu TN_{cr}} zt \tag{13}$$

in the time interval $0 < t < \tau$. In deriving Eq. (13), the transit time through the deflection has been neglected. Equation (13) is the equation for a linearly ramped streak camera.

Although beyond the scope of this paper, it is possible to show the thickness T can be kept small by using total internal reflection from the upper surface and that free-carrier absorption can be minimized by the appropriate choice of semiconductor, etc. We believe that such a plasma-beam deflector could lead to the first practical streak camera for the infrared.

*Present address, University of Toronto, Toronto, Ontario, Canada.

REFERENCES

1. A. J. Alcock and P. B. Corkum, "Ultra-fast switching of infrared radiation by laser-produced carriers in semiconductors," Can. J. Phys. **57**, 1280–1290 (1979).
2. A. J. Campillo, R. C. Hyer, and S. L. Shapiro, "Broadly tunable picosecond infrared source," Opt. Lett. **4**, 325–327 (1979).
3. T. Elsaesser, A. Seilmeier, W. Kaiser, P. Koidl, and G. Brandt, "Parametric generation of tunable picosecond pulses in the medium infrared using AgGaS crystals," Appl. Phys. Lett. **44**, 383–385 (1984).
4. H. S. Kwok and E. Yablonovitch, "30-psec CO_2 laser pulses generated by optical free induction decay," Appl. Phys. Lett. **30**, 158–160 (1977); E. Yablonovitch and J. Goldhar, "Short CO_2 laser pulse generation by optical free induction decay," Appl. Phys. Lett. **25**, 580 (1974).
5. J. Lucas, "Infrared fibres," presented at the Third International Conference on Infrared Physics, ETH-Zurich, Switzerland, July 23–27, 1984.
6. It is interesting to note that N_{cr} can be strongly modulated by free-carrier mass changes. In many semiconductors, large mass changes can be produced by the Gunn effect.
7. R. A. Fisher and B. J. Feldman, "Generation of single ultrashort CO_2 laser pulses in a Fabry–Perot interferometer," Opt. Lett. **1**, 161–163 (1977).
8. See, for example, *Optical Bistability*, C. M. Bowden, M. Ciftan, and H. R. Robl, eds. (Plenum, New York, 1980).
9. P. B. Corkum, "High-power, subpicosecond 10 μm pulse generation," Opt. Lett. **8**, 514–516 (1983).
10. D. H. Auston, R. P. Smith, A. M. Johnson, W. M. Augustiniak, J. C. Bean, and D. B. Fraser, "Recent advances in picosecond optoelectronics," in *Picosecond Phenomena II*, R. M. Hochstrasser, W. Kaiser, and C. V. Shank, eds., Vol. 14 of Springer Series in Chemical Physics (Springer-Verlag, Berlin, 1980), pp. 71–74.
11. S. W. Thomas, "Crystal streak camera," Proc. Soc. Photo-Opt. Instrum. Eng. **97**, 73–79 (1976).
12. M. B. Chang, "Total internal reflection deflector," Appl. Opt. **21**, 3879–3883 (1982).